Multiscale and Multidisciplinary Modeling, Experiments and Design
https://doi.org/10.1007/s41939-024-00520-5

ORIGINAL PAPER

# Investigation of dry sliding wear characteristics of Al 7075 reinforced with SiC-graphite hybrid composites: multi-parameter optimization using grey relational analysis

**Atla Sridhar[1] · Nagavelly Shiva Kumar[2] · K. Prasanna Lakshmi[3] · CH. V. Satyanarayana Raju[4]**

Received: 15 May 2024 / Accepted: 22 June 2024


**Abstract**
Metal matrix composites made of aluminium and ceramics reinforced with silicon carbide (SiC) have desirable mechanical characteristics. On the other hand, ceramic composites made of aluminium may need improvement in their lubricating and tribological properties. This study aims to develop a new material utilizing the powder metallurgy (P/M) technique by incorporating Graphite (Gr), which is self-lubricating. This research investigated the impact of Graphite on the wear characteristics of a hybrid composite material composed of Al 7075/SiC and varying percentages of Graphite (X = 0, 5, and 10 weight %). An experimental study was conducted to analyze the mechanical and wear properties of the hybrid composite. The hardness of Al7075 increased by 5% with 5 wt.% SiC compared to the base alloy. Adding 5 wt.% graphite to the Al7075/5 wt.% SiC composite increased hardness by 2.7% compared to the base alloy, but with 10 wt.% graphite, the hardness decreased below the base alloy. This decrease is likely due to graphite agglomeration, softer phases, and poor interfacial bonding. The wear characteristics of the composite were tested using the pin-on-disc method. Scanning electron microscopy (SEM) analysis of the hybrid composite revealed that the reinforcement particles were evenly distributed throughout the matrix. The tribological behaviour was optimized using the Taguchi design of experiments and the grey relational technique. The results showed a reduction in wear loss of around 25.08% and a reduction of the friction coefficient of about 54.37%. The results demonstrated that the hybrid composite composed of Al7075 with 5 wt.% SiC and 5 wt.% graphite outperformed the other hybrid composites regarding mechanical and tribological characteristics.

**Keywords** Hybrid composites · Powder metallurgy · Multi-objective optimization · Design of experiments · Al 7075 · Wear properties · Graphite

## 1 Introduction

Its high elongation at failure, high tensile strength, yield strength, and strength-to-weight ratio make AA7075 attractive for various automotive, mechanical, aerospace, marine and defence applications. As previously stated, AA 7075 is extensively used in several sectors, either on its own or as a metal matrix composite. For these reasons, AA7075 was Selected as a matrix material for this study. On the other hand, it has a lot of major drawbacks, such as a complicated welding procedure and a high reactivity to caustic acids, oxygen, and water. Typically, powder metallurgy or stir casting creates aluminium matrix composites (Venkatesh and Deoghare 2022; Rao and Srinivas 2023; Manoj et al. 2022; Ibrahim et al. 2016). The stir-casting method uniformly distributes the particles throughout the liquid metal before casting and solidification (Rohatgi et al. 2020; Prasad

✉ Atla Sridhar
atla.sridhar9@gmail.com

1 Department of Mechanical Engineering, Gitam School of Technology, Rudraram, Hyderabad, Telangana 502329, India

2 Department of Mechanical Engineering, VNR Vignana Jyothi Institute of Engineering and Technology, Hyderabad, Telangana 500 090, India

3 Department of Mechanical Engineering, Jawaharlal Nehru Technological University Hyderabad, Hyderabad, Telangana 500085, India

4 Control Systems Laboratory, Research Center Imarat, Defence Research and Development Organisation, Hyderabad, Telangana 500069, India

Published online: 15 July 2024

and Shoba 2014). The research was carried out on an aluminium matrix created using the stir casting technique and was reinforced with various amounts of silicon carbide (SiC) (Sijo and Jayadevan 2016). Maximum hardness and tensile strength were observed at 20 wt.% SiC. Titanium carbide (TiC) particles were reinforced, with Al7075 alloy as the base metal (Rao et al. 2016). Wear characteristics with 8 wt.% TiC were better than those with other composites and matrix metals when using the stir-casting process (Rao et al. 2016). It follows that the addition of reinforcing ceramic particles enhanced the mechanical qualities. In addition to experimenting with Al7075 alloy, the researchers looked at Al6061 alloys; a particularly noteworthy study compared the mechanical characteristics of Al6061-SiC and Al6061-SiC/graphite hybrid composites. Mechanical characteristics, density, and microstructural investigations define the manufactured composites. Findings showed that Al6061 alloy's distributed Graphite and SiC improved composites' tensile strength (Gugulothu et al. 2023). Composites made using the stir casting method and containing the following proportions of SiC(7.5, 10 wt%), Fly Ash (7.5 wt%), $Al_2O_3$ (0.5 wt%), and $B_4C$ (0%,3%, 5 wt %) were subsequently investigated for their wear properties. The wear resistance of these hybrid composites increases as the percentage of $B_4C$ increases, making them superior to single-reinforced composites (Paulraj et al. 2021). An Al alloy reinforced with $Al_2O_3$, $B_4C$, and SiC showed increased mechanical characteristics (Topcu et al. 2009). According to the research above, improving the mechanical characteristics of the basic alloy is as simple as adding ceramics like $TiO_2$, $B_4C$, or $Al_2O_3$. $B_4C$ has exceptional interfacial bonding properties. Ceramics are not the only acceptable material for reinforcements; cast iron is one example of a metal. According to research, wear resistance mechanical properties were all enhanced in Al7075, reinforced with grey cast iron and fly ash, produced using stir casting (Singh and Kumar 2022). Among the ceramics mentioned earlier and current works, SiC is prominent because of its exceptional mechanical characteristics. There was a study on the mechanical properties, microstructure, and wear characteristics of SiC-reinforced aluminium matrix composites (AMCs). An AMC reinforced best-achieved results for wear resistance, tensile strength, and compressive strength with 7 wt.% SiC (Bharathi and Kumar 2023). Chemically strengthening a base metal with SiC greatly enhances its mechanical and wear properties (Kalsi et al. 2019). As shown in another case, adding 6% TiC to Al7075 improved its mechanical qualities and corrosion resistance (Krishna Prasad et al. 2022; Ravi et al. 2018).

Because of the fantastic outcomes that may be achieved by implementing two or more ceramics with different concentrations, the choice was made to use a hybrid composite rather than regular reinforcement (Ande et al. 2019; Singh and Gautam 2019). It has been studied and compared the mechanical and tribological properties of Al-molybdenum disulfide ($MoS_2$) composites to those of Al-Si10Mgalloy, an aluminium alloy known for its amazing wear resistance. Because $MoS_2$ was added, the composite's density and hardness increased and its ultimate tensile strength decreased (Rebba and Ramanaiah 2014; Basavarajappa et al. 2017).Al7075 is ideal for piston applications because of its extreme stress and strain resistance caused by its very high Si concentration (Devaganesh et al. 2020). However, because of its low density, Al7075 becomes hotter more quickly and softens when it comes into touch with other metals, which increases its wear rate (Kumar et al. 2018). Al7075 alloys are fortified with solid lubricants to avoid this problem. Composites made of aluminum with graphene exhibit enhanced toughness, elasticity, and tensile strength. Some authors discovered that Graphene and graphite enhance the wear and friction properties of composites by using methods such as solid lubrication and the development of transfer films. The layered structure of graphene enables effortless shearing, leading to a decrease in friction and wear, particularly in situations involving dry sliding (Berman et al. 2014). Graphite deposits a protective coating on surfaces upon contact, reducing direct metal-to-metal interaction and improving resistance to wear across different levels of load (Doddamani et al. 2017; Kumar 2018).

Since no prior research has examined the effects of mixing SiC with various weight percentages of Graphite (Gr) and their fabrication process using the powder metallurgy (P/M) route. An effort is made in this study to examine the effect of Graphite on the wear behaviour of a hybrid composite material made of Al 7075/SiC and X Wt.% graphite (where X = 0, 5, and 10%) to create a novel material using the powder metallurgy (P/M) process. It generates optimal parameters for wear loss and friction coefficient in regular optimization methods. Wear loss and friction coefficient must be optimized to get the common standard parameters for both quality metrics. Hence, Simultaneous optimization is carried out using Taguchi-Grey relational analysis to get the common standard parameters.

## 2 Methodology

### 2.1 Sample Preparation

The main objective of this study was to develop Al 7075- 5 Wt. % SiC- X Wt.% Gr (X = 0, 5, and 10)hybrid composites using (P/M) technique to improve mechanical characteristics and reduce wear. The chemical composition of a matrix material, Al7075 alloy, is detailed in Table 1. A mixture of 25 μm silica particles and 1 μm graphite were used as reinforcements.

**Table 1** Al7075 Chemical composition

| Elements | Cu | Si | Mg | Fe | Mn | Zn | Ni | Cr | Ti | Al |
|---|---|---|---|---|---|---|---|---|---|---|
| % | 1.62 | 0.06 | 2.54 | 0.19 | 0.075 | 5.63 | 0.05 | 0.23 | 0.048 | Bal |

A constant weight of 5% SiC and a weight percentage of (X = 0–5–10%) graphite reinforment particles were used to make the hybrid composites. The samples were prepared using a P/M route to ensure the reinforcing particles were evenly distributed. Prabhu Copper Ltd., located in Mumbai, India, was the source of these metal powders. A total of 2,000 grammes of Al 7075 alloy, 1,000 of SiC, and 500 of Gr.

The moisture is removed from all powders by preheating them in a muffle furnace at 110 °C for 1.25 h before the operation begins (Daver et al. 1988). Next, a specific mixture of powders was ground in a planetary ball mill. The milling operation took up to 60 h and used tungsten bowls with balls ranging from 10 to 50 mm. The powder-to-ball weight ratio was 1:10 (Koli et al. 2014). Figure 1a–c shows that the blending and typical grinding processes were carried out at 300 rpm in a toluene medium to avoid oxidation and powder adhering to the vial wall (Gupta et al. 2017).

Universal testing equipment compacted the thoroughly mixed powders at 700 MPa pressure and 70 kN applied stress. Zinc stearate was used before each test to ensure the smooth operation of the die walls during the loading and ejecting of the sample from the die (Schneider 2003). Samples that are green-compacted are then formed. The prepared samples were vacuum sintered at 600 °C in a tube furnace operating under vacuum. After vacuuming, the starting temperature rises from 0 to 300 °C over 100 min at an average 3 °C/min rate. Subsequently, they were allowed to soak in a solution at about 300 °C for 100 min. The duration of the heating process from 300 to 600 °C is 100 min. After soaking it for 120 min at 600 degrees Celsius, let it cool until it reaches ambient temperature, as shown in Fig. 2a, b (Upadhyaya 1997). Subsequently, samples are manufactured using various classifications of emry papers.

## 2.2 Density and hardness measurement

Archimedes' principle was considered while measuring the density of the created hybrid composites utilizing a state-of-the-art electronic weighing machine with an accuracy of 0.0001 mg (Arya et al. 2023). The porosity of the Al7075-SiC-graphite hybrid composite was assessed by initially weighing the samples in air before being immersed in distilled water to determine their submerged weight. The porosity has been calculated using the difference between these weights, taking into consideration the density of water. Additionally, the composite's hardness is measured using a Rockwell hardness method. Table 2 shows the mechanical characteristics of the samples. The mechanical and tribological characteristics may be fine-tuned by adjusting the graphite content while maintaining a constant SiC content.

$$\text{Porosity} = \frac{(w_i - w_d)}{(w_i - w_s)}$$

## 2.3 Microstructure characterization

At the end of 60 h in the ball mill, the powders had an average size of 200 nm. Microscopic examination of the powder shows that the Al7075, SiC, and Graphite are evenly distributed. To study the microstructural behaviour of the samples, they were cut into sections and treated using the principles of metallographic technique. Microstructural analysis is vital for investigating and ensuring product quality, so a scanning electron microscope (SEM) was used. Regular hand polishing procedures utilizing silicon carbide sheets of varied grits (200–1200) have been used to smooth out the metallographically generated samples. Afterwards, the samples are fine-ground and polished to a mirror finish using a distilled water solution containing 01 μm diamond paste. An etch-polish-etch procedure was used to get the best microstructural features (Mohan and Ramesh Babu 2011; Heard 2021). The grain structure and reinforced particles of varying sizes, shapes, and distributions were established through a microscope. The SEM micrographs show that these particles are evenly dispersed throughout the Al 7075 matrix.

## 2.4 Dry sliding wear test

A series of dry sliding wear studies have been conducted as per the ASTM standard G99-05 (Hong et al. 2017). The pin-on-disc machine for evaluation purposes. EN31 steel is used to make counter disc. In preparation for the experiment, the cylindrical samples and the disc were cleaned with acetone (Hong et al. 2017). Each experiment subjected Prepared hybrid-composite samples to loads between 5 and 15 N. The studies were conducted over 1000–2000 m, with sliding speeds ranging from 1–3 m/s. We used organic substances to scrub the surfaces of the counter and specimens completely after every experiment to remove any evidence of the chemicals. The pin is measured before and after the inspection to within 1 X $10^{-4}$ g of error to determine the amount of wear loss. The strain-gauge load measurements were used to

**Fig. 1** **a** Powders in tungsten vials before milling. **b** High Energy Ball Milling. **c** Powders in vials after 60 h milling

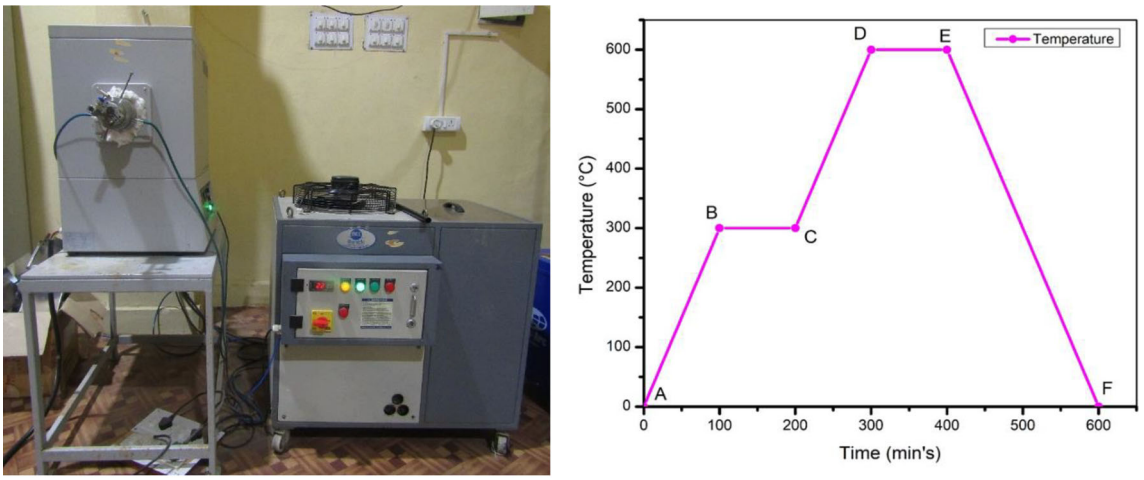


**Fig. 2** **a** A Vacuum sintering equipment. **b** Process for vacuum sintering

**Table 2** Density and Hardness Measurement

| Sample number | Composition of materials | Porosity (%) | Experimental density (g/cc) | Theoretical density (g/cc) | Hardness (HRB) |
|---|---|---|---|---|---|
| 1 | Al7075 | 1.0677 | 2.78 | 2.81 | 73 |
| 2 | 95% Al7075 + 5% SiC + 0% Gr | 1.0601 | 2.80 | 2.83 | 77 |
| 3 | 90% Al7075 + 5% SiC + 5% Gr | 1.786 | 2.75 | 2.80 | 75 |
| 4 | 85% Al7075 + 5% SiC + 10% Gr | 2.166 | 2.71 | 2.77 | 70 |

compute the friction coefficient (Stachowiak and Stachowiak 2001). The replies from each run were averaged and recorded in the table since all tests were repeated three times.

## 2.5 Design of experiments

Investigating using Taguchi's method is smart since it is efficient, rational, and takes little time. Providing detailed information about the factors and their levels will enhance the clarity of the "Design of Experiment" section. Specifically, we have detailed the factors and their respective levels as follows: the weight percentage of graphite with levels at 0 wt%, 5 wt%, and 10 wt%; the load with levels at 5 N, 10 N, and 15 N; the sliding distance with levels at 1000 m, 1500 m, and 2000 m; and the speed with levels at 1 m/s, 1.5 m/s, and 2 m/s. The Taguchi method was selected for its efficiency in studying the effect of multiple factors with a minimal number of experiments, using an L27 orthogonal array to design the

**Table 3** Taguchi ($L_{27}$) experiments and S/N readings

| S. no | Sliding Speed | Reinforcement (% of Gr.) | Sliding distance | Load (N) | Wear loss (g) | COF | SNRA1 | SNRA2 |
|---|---|---|---|---|---|---|---|---|
| 1 | (m/s) | 0 | (X × 103 m) | 5 | 0.00850 | 0.144 | 41.411 | 16.802 |
| 2 | 1 | 0 | 1 | 5 | 0.00982 | 0.164 | 40.175 | 15.687 |
| 3 | 2 | 0 | 1.5 | 5 | 0.01051 | 0.171 | 39.576 | 15.299 |
| 4 | 3 | 0 | 2 | 10 | 0.00964 | 0.181 | 40.354 | 14.836 |
| 5 | 2 | 0 | 1 | 10 | 0.01192 | 0.194 | 38.489 | 14.226 |
| 6 | 3 | 0 | 1.5 | 10 | 0.02031 | 0.152 | 33.850 | 16.317 |
| 7 | 1 | 0 | 2 | 15 | 0.00877 | 0.203 | 41.209 | 13.820 |
| 8 | 3 | 0 | 1 | 15 | 0.01455 | 0.180 | 36.772 | 14.889 |
| 9 | 1 | 0 | 1.5 | 15 | 0.01624 | 0.190 | 35.809 | 14.406 |
| 10 | 2 | 5 | 2 | 5 | 0.00372 | 0.148 | 48.636 | 16.542 |
| 11 | 2 | 5 | 1 | 5 | 0.00429 | 0.161 | 47.535 | 15.858 |
| 12 | 3 | 5 | 1.5 | 5 | 0.01333 | 0.135 | 37.523 | 17.354 |
| 13 | 1 | 5 | 2 | 10 | 0.00421 | 0.149 | 47.535 | 16.495 |
| 14 | 3 | 5 | 1 | 10 | 0.01120 | 0.142 | 39.015 | 16.948 |
| 15 | 1 | 5 | 1.5 | 10 | 0.01344 | 0.144 | 37.457 | 16.778 |
| 16 | 2 | 5 | 2 | 15 | 0.00673 | 0.186 | 43.478 | 14.595 |
| 17 | 1 | 5 | 1 | 15 | 0.01050 | 0.198 | 39.576 | 14.044 |
| 18 | 2 | 5 | 1.5 | 15 | 0.01217 | 0.203 | 38.344 | 13.841 |
| 19 | 3 | 10 | 2 | 5 | 0.00195 | 0.161 | 54.424 | 15.820 |
| 20 | 3 | 10 | 1.0 | 5 | 0.01033 | 0.156 | 39.743 | 16.131 |
| 21 | 1 | 10 | 1.5 | 5 | 0.01052 | 0.165 | 39.576 | 15.624 |
| 22 | 2 | 10 | 2 | 10 | 0.00751 | 0.170 | 42.498 | 15.380 |
| 23 | 1 | 10 | 1 | 10 | 0.00812 | 0.173 | 41.830 | 15.239 |
| 24 | 2 | 10 | 1.5 | 10 | 0.01294 | 0.175 | 37.788 | 15.099 |
| 25 | 3 | 10 | 2 | 15 | 0.00732 | 0.181 | 42.733 | 14.827 |
| 26 | 2 | 10 | 1 | 15 | 0.01091 | 0.201 | 39.251 | 13.931 |
| 27 | 3 | 10 | 1.5 | 15 | 0.01611 | 0.214 | 35.863 | 13.680 |

experiments. Reading responsive components about certain levels is the primary practical effect. The size of the levels of its factors determines the overall average response. Finding the best factor-to-response formulations and improving performance are the goals of the technique's design (Girish et al. 2016; Arunkumar et al. 2020). The Signal/Noise ratio (S/N) is produced from meticulously studied and converted testing data. For each property, it offers a unique signal-to-noise ratio (S/N). Three kinds of S/N ratio characteristics are included: lowest, maximum, and nominal best. Once again, the low frictional and wear coefficients are a plus. The S/N transformation is transformed into a logarithmic model using mathematical means, as may be shown below. The observed data is denoted by y for every 'n' data point. The three-stage examination of the four primary affecting factors is shown in Table 3. Table 4 shows the tribological findings that were used to perform the tests. It was used to construct the main effects plot, and ANOVA produced the contributing findings (Saurabh et al. 2022).

## 3 Results and discussion

### 3.1 Microstructure characterization

Figure 3a–d shows scanning electron microscopy (SEM) pictures of sintered Al7075 samples. Compacted and sintered Al7075 morphologies with different percentages of Graphite and silicon carbide exhibit robust chemical bonds. A closer look at these microscopic formations revealed cubic silicon carbide particles and graphite flakes. The Al7075 metal matrix had graphite-reinforced and silicon carbide-coated particles evenly distributed within. Figure 3c, d demonstrate that the SiC and Gr particles were evenly distributed

**Table 4** ANOVA for wear loss

| Source | DF | Adj MS | Adj SS | P-Value | F-Value | Contribution (%) |
|---|---|---|---|---|---|---|
| Sliding Distance (m) | 2 | 0.000124 | 0.000248 | 0.000 | 94.57 | 55.98 |
| Load (N) | 2 | 0.000030 | 0.000059 | 0.000 | 22.65 | 13.31 |
| Sliding Velocity (m/s) | 2 | 0.000027 | 0.000053 | 0.000 | 20.33 | 11.96 |
| Reinforcement (wt. % of Gr) | 2 | 0.000030 | 0.000059 | 0.000 | 22.55 | 13.31 |
| Error | 18 | 0.000001 | 0.000024 | | | 5.41 |
| Total | 26 | | 0.000443 | | | |

S = 0.001145, R-Sq = 94.67% and R-Sq (adj) = 92.30%

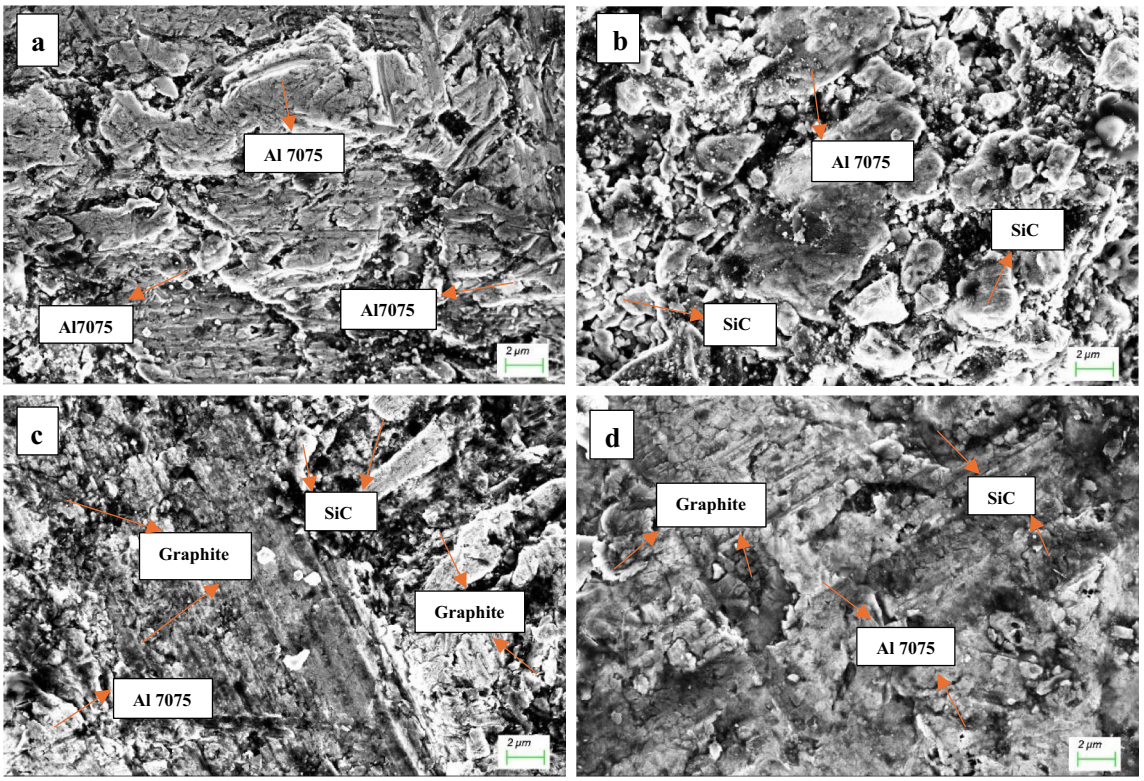


**Fig. 3** Microstructure: **a** Al 7075, **b** Al 7075–5 wt.% SiC-0 wt.% Gr, **c** Al 7075–5 wt.% SiC-5 wt.% Gr, **d** Al 7075–5 wt.% SiC-10 wt.% Gr

throughout the Al7075 matrix. This feature claims that variables including milling speed, period, charge ratio, milling medium, and sintering method are responsible for the superb SiC and Gr particle distribution in the Al7075 matrix (Bhoi et al. 2020). They were also mixed to ensure the Al7075 powder and reinforcing particles formed a strong chemical connection before sintering.

## 3.2 Density measurement

The rule of mixtures is used to derive theoretical densities from volume fractions and component densities, whereas Archimedes' principle determines experimental densities. Table 2 lists the density and porosity of several composite materials with variable weight% of reinforcement. The discrepancy between the theoretical and actual findings in Fig. 4 illustrates the impact of ceramic and solid lubricant reinforcements on the density of various composite materials, as shown in Table 2. Compared to the basic alloy (Al7075) and the Al7075/5wt% SiC composite, the density of the Al7075/10-Wt.% Gr hybrid composite is lower. When compared to Al7075/5wt% SiC and Al7075/5-Wt.% SiC/10-Wt.% Gr, the hybrid composite with these proportions, has a lower density than base alloy material but a greater density than Al7075/5wt% SiC. This is because the composites, as mentioned above, have a lower proportion of Al7075 (2.81 g/cc) and a larger amount of Graphite (2.26 g/cc).The

density of the Al7075/5-Wt.% SiC/10-Wt.% Gr hybrid sample is 2.71 g/cc, whereas the density of the Al7075/5-Wt.% SiC composite is 2.8 g/cc, according to Table 2. This is because the composites include SiC, a reinforcing material with a greater density. As graphite concentration grows, SiC particles lose their solid solution strengthening and load transmission effects, making them less effective (Jamwal et al. 2020).

### 3.3 Hardness measurement

Table 2 shows the hardness values of the hybrid composite samples with varying weight percentages of reinforcements. Tabulated values are the average hardness values from three separate tests. Rockwell hardness tests performed on Al7075/5-Wt.% SiC/X-Wt.% Gr-(X = 0, 5, and 10) composites. Compared to the base alloy, the hardness values of the hybrid composite samples made of Al7075/5-Wt.% SiC/10-Wt.% Gr are lower. The hardness rises between 0% SiC and 5% SiC composites, but the hardness falls between 0% Gr and 10% Gr hybrid composites. Adding SiC particles causes the hardness ratings to rise. Adding SiC to the composite material increases its hardness by preventing the migration of dislocations, which causes the matrix alloy to deform under stress. Figure 5 shows that when the SiC concentration in composite samples rises, their hardness also increases. The composite sample made of Al 7075 and 5 wt.% SiC has a maximum hardness enhancement of 5.4%. Composites made from aluminium with ceramic particles, such as SiC, added to the matrix make the final product harder. The layers of graphite structure in hybrid composites experience modest Vander Wall forces. The external load may be supported by sliding the graphite layers over each other (Sharma et al. 2019; Akhtar 2021; Holmberg and Matthews 2009). As the graphite percentage increases from 0 to 10%, the hardness values in Fig. 5. Since SiC restricts dislocation movement, it may harden the Al7075 matrix. However, graphite does not help this process. Hardening composites requires load transmission from matrix to reinforcement (SiC). Because graphite is soft and lubricating, increasing its amount diminishes composite hardness, load-bearing capacity, and transmission. Adding 5 wt.% graphite to the Al7075/5 wt.% SiC composite increased hardness by 2.7% compared to the base alloy. However, the hardness decreased below the base alloy level with 10 wt.% graphite. This decrease is likely due to graphite agglomeration, the introduction of softer phases, and weakening of interfacial bonding.

### 3.4 Dry sliding wear

At three different levels, the four process parameters were examined. The combinations provided in Table 3 were used to conduct the experiments. Minitab 2020 was used to create main effect plots, and an ANOVA was performed to determine the significance of the testing parameter.

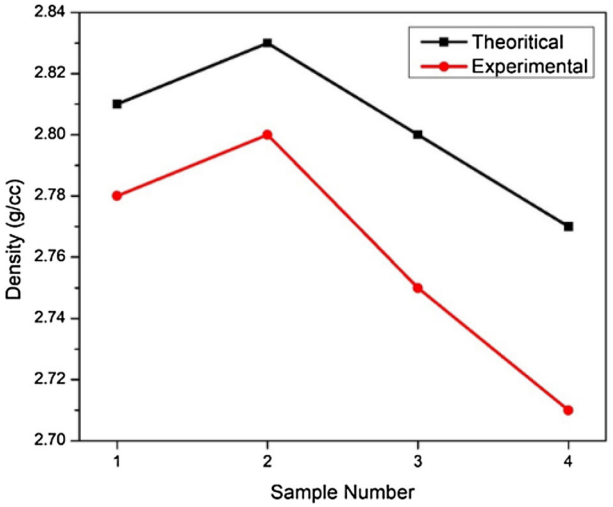


**Fig. 4** Density

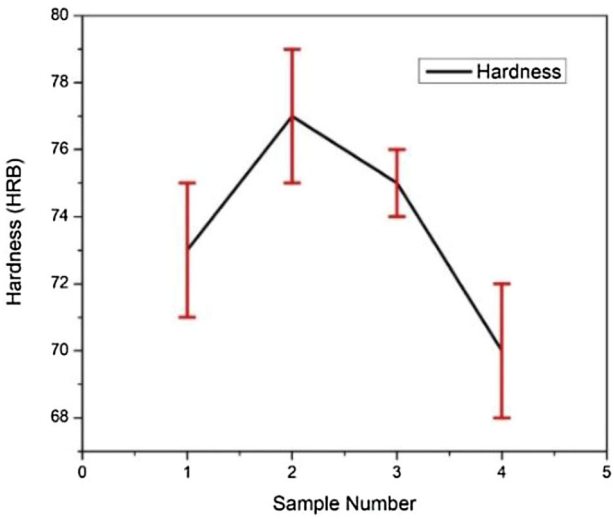


**Fig. 5** Hardness

### 3.5 Analysis of factors for wear loss

To examine the combined impact of A (reinforcement, in percentage of Gr.), B (load, in N), C (slide distance, in m), and D (sliding speed, in m/s), on wear loss, an ANOVA analysis was conducted. A 5% threshold of significance was used for this research. Table 4 displays the relative importance of the parameters, including reinforcing weight (p = 13.31%), load (p = 13.31%), the Distance of sliding (p = 55.98%), and velocity of sliding (p = 11.96%). Sliding Distance is one of the parameters that substantially affects wear loss (p = 55.98%).

Standard error (S) represents the dispersion of measured wear loss values around regression model predictions.A standard error of 0.0011447 demonstrates modest wear loss variability around the regression line. The accuracy with which our model predicts wear loss improves the dependability of our experimental findings and forecasts. (R-Sq) Determination Coefficient: The independent factors in the model explain 94.67% of wear loss variability, according to an R-Sq value of 94.67%. This high number validated the experimental method, which shows that material composition and manufacturing conditions strongly affect wear loss. R-Squared (adj): This model's modified R-Sq of 92.30% compensates for predictors and sample size, proving its wear loss prediction despite its complexity. It improves our model's capacity to capture the crucial interactions between independent factors and wear loss.

#### 3.5.1 Effect of parameters on wear loss

Figure 6 displays the primary effect plot of composite wear loss as a function of various factors. The major effect graphic remains unaffected if the parameter value stays near the horizontal line. When plotting the primary effect, a steeper parametric line indicates that the parameter has a greater impact. Although all three parameters—load, speed, and reinforcement weight percentage—are important, the main effect plot reveals that parameter C—sliding distance—has the most impact. More asperity-to-asperity contact time and a larger actual contact area resulted from a longer sliding distance, which accelerated wear on the composites and contributed to the development of wear debris. More contact duration between asperity-asperity and an enhanced contact area results from increased sliding Distance, which adds to increased wear on composites. With increased load and sliding Distance, wear loss has been enhanced, suggesting that the material is becoming increasingly separated from the sample base (Zhai et al. 2021; Sawyer et al. 2014). In addition, the worn base forms a thick tribo layer of Graphite, which reduces wear. Incorporating extra contact regions reduces wear. Across the board, the 5% hybrid composite outperformed the other two options (0% and 10%) regarding wear performance.

### 3.6 Analysis of factors for COF

An ANOVA analysis was conducted to examine how different factors collectively affected the coefficient of friction. The coefficient of friction was considerably affected by the load (61.25%), as shown in Table 5. Conversely, the coefficient of friction was less affected by the proportion of graphite reinforcing weight (8.7%). Therefore, the results of this investigation demonstrated that the sliding Distance significantly impacts wear loss. Another important consideration when calculating the coefficient of friction is the load. Wear loss and coefficient of friction (COF) seemed to help the 13.31% and 8.7% graphite weight percentages, respectively.

$S = 0.0011447$, R-Sq = 94.67% and R-Sq (adj) = 92.30%.

#### 3.6.1 Effects of parameters on COF

The coefficient of friction was most affected by the applied weight. In contrast, sliding speed and % of Graphite were only marginally relevant, as shown in Fig. 7. the friction doesn't change across all composite materials as the sliding distance increases. As the weight % of the composite rises, its coefficient of friction also increases significantly. Due to the quick degradation of the graphite layer caused by a fast rise in applied stress, the layer is more robust at lower loads than higher ones. The coefficient of friction drops as the weight percentage of Graphite rises to a certain point, which is 5%. As the proportion of Graphite in the overall weight grows, it eventually rises. This is because the Al7075/5%SiC composite contains graphite, a powerful lubricant that reduces friction by causing a layer of the lubricant-rich substrate to accumulate on the tribo-surface. Friction wears surfaces at an increasing rate when the proportion of Graphite in the total weight is more than 5%. The oxide layer has more surface fractures, which deteriorates worn surfaces. Surfaces that are sliding against each other may cause abrasion.

Composites may adhere to the counter surface as a consequence. So, the coefficient of friction is always going up because adhesion is constantly going up. For the lowest wear loss, the ideal parameter settings were 5 wt. % graphite reinforcement, 5 N load, 1000 m sliding distance, and 3 m/s sliding velocity. In addition, When the graphite reinforcement is 5 weight %, the load is 5 Newtons, the sliding Distance is 1000 m, and the speed is 1 m per second, the minimal coefficient of friction is obtained. The wear loss and friction coefficient optimum values it produced were varied. To determine the shared optimal values for both quality parameters, it is necessary to optimize both reactions, namely wear loss and coefficient of friction. Taguchi-Grey relational analysis performs simultaneous optimization (Ikubanni et al. 2021; Gajalakshmi et al. 2019).

### 3.7 Grey relational analysis

The Taguchi technique is among the most popular choices when optimizing cost and quality. A performance variance is evaluated concerning the target result using the Taguchi technique. This variation is used to construct a loss function. Given that total noise elimination is impossible, the Taguchi method employs a robustness concept to assess the ideal level of important controllable variables while simultaneously attempting to mitigate noise impacts. The Taguchi

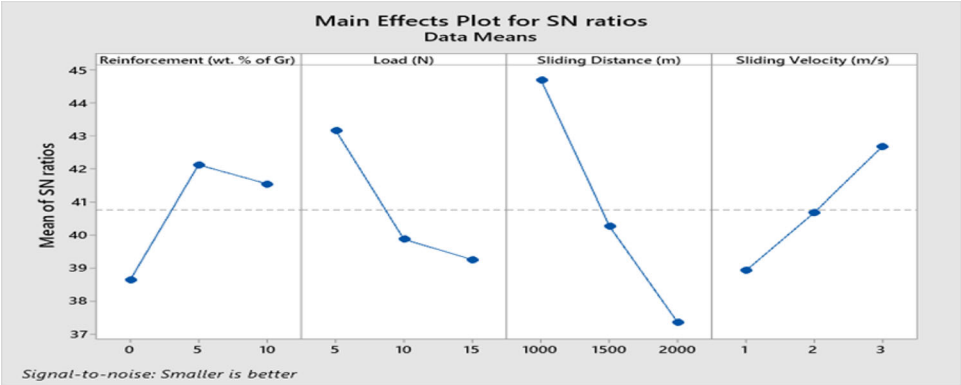


**Fig. 6** Main effects plot for Wear loss

**Table 5** ANOVA for COF

| Source | DF | Adj MS | Adj SS | P-value | F-value | Contribution (%) |
|---|---|---|---|---|---|---|
| Load (N) | 2 | 0.003596 | 0.007192 | 0.000 | 29.32 | 61.25 |
| Reinforcement (wt. % of Gr) | 2 | 0.000511 | 0.001023 | 0.033 | 4.17 | 8.7 |
| Sliding Distance (m) | 2 | 0.000052 | 0.000103 | 0.663 | 0.42 | 0.87 |
| Sliding Velocity (m/s) | 2 | 0.000608 | 0.001215 | 0.019 | 4.95 | 10.35 |
| Error | 18 | 0.000123 | 0.002208 | | | 18 |
| Total | 26 | | 0.011741 | | | |

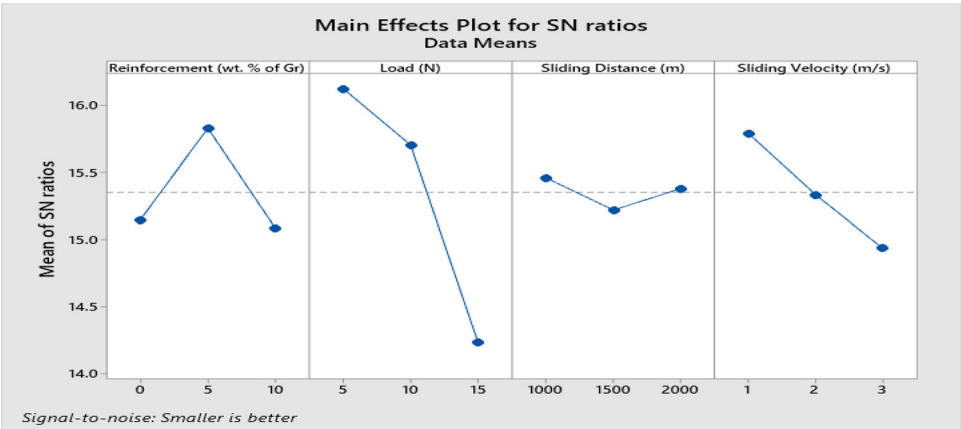


**Fig. 7** Main effects plot for coefficient of friction

method incorporates a novel orthogonal array architecture to examine these characteristics using several tests. In order to determine the best level of management for several variables at once, the Grey relational analysis method is used. Following are the steps that were followed when the grey relational analysis technique was put into action:

First Step: In a grey relational investigation, the experimental outcomes corresponding to the output result (ranging from 0 to 1) are normalized. If the goal value of the real sequence is infinite, then it has the "higher is better" quality.

$$X_{ij} = \frac{(Y_{ij}) - min(Y_{ij})}{max(Y_{ij}) - min(Y_{ij})}$$

When its original sequence's goal function is zero, it has the "smaller-the-better" properties.

$$X_{ij} = \frac{max(Y_{ij}) - (Y_{ij})}{max(Y_{ij}) - min(Y_{ij})}$$

In this case, the $j_{th}$ answer is used to get the findings for the $i_{th}$ experiment and $X_{ij}$ and $Y_{ij}$ are the standardized data. In the replies, min $(Y_{ij})$ represents the lowest value and max $(Y_{ij})$ represents the highest value. Here, the "smaller is better" principle should be used to minimize wear loss and coefficient of friction. Table 6 displays the normalized data.

Secondly, after the pre-processing of the findings, the following may be said about the $j_{th}$ response characteristics of

**Table 6** Taguchi Grey relation normalisation

| Experiment. No | COF | Wear loss (g) | Normalisation | |
|---|---|---|---|---|
| | | | COF | Wear loss (g) |
| 1 | 0.1445 | 0.0085 | 0.887 | 0.678 |
| 2 | 0.1643 | 0.0098 | 0.635 | 0.603 |
| 3 | 0.1718 | 0.0105 | 0.539 | 0.563 |
| 4 | 0.1812 | 0.0096 | 0.420 | 0.615 |
| 5 | 0.1944 | 0.0119 | 0.252 | 0.483 |
| 6 | 0.1528 | 0.0203 | 0.781 | 0.000 |
| 7 | 0.2037 | 0.0087 | 0.134 | 0.667 |
| 8 | 0.1801 | 0.0145 | 0.434 | 0.333 |
| 9 | 0.1904 | 0.0162 | 0.303 | 0.236 |
| 10 | 0.1489 | 0.0037 | 0.831 | 0.954 |
| 11 | 0.1611 | 0.0042 | 0.676 | 0.925 |
| 12 | 0.1356 | 0.0133 | 1.000 | 0.402 |
| 13 | 0.1497 | 0.0042 | 0.821 | 0.925 |
| 14 | 0.1421 | 0.0112 | 0.917 | 0.523 |
| 15 | 0.1449 | 0.0134 | 0.882 | 0.397 |
| 16 | 0.1863 | 0.0067 | 0.355 | 0.782 |
| 17 | 0.1985 | 0.0105 | 0.200 | 0.563 |
| 18 | 0.2032 | 0.0121 | 0.140 | 0.471 |
| 19 | 0.1618 | 0.0029 | 0.667 | 1.000 |
| 20 | 0.1561 | 0.0103 | 0.739 | 0.575 |
| 21 | 0.1655 | 0.0105 | 0.620 | 0.563 |
| 22 | 0.1702 | 0.0075 | 0.560 | 0.736 |
| 23 | 0.1730 | 0.0081 | 0.524 | 0.701 |
| 24 | 0.1758 | 0.0129 | 0.489 | 0.425 |
| 25 | 0.1814 | 0.0073 | 0.417 | 0.747 |
| 26 | 0.2011 | 0.0109 | 0.167 | 0.540 |
| 27 | 0.2142 | 0.0161 | 0.000 | 0.241 |

the $i_{th}$ experiment:

$$GRC = \frac{(\Delta_{\min}) + (\gamma \Delta_{\max})}{\left(\Delta_{i(k)}\right) + (\gamma \Delta_{\max})}$$

In cases when The reference sequence is represented by $Y_{ij}$ in this context. The set of all possible comparisons is $X_{ij}$. The absolute value difference between $Y_{ij}$ and $X_{ij}$ is represented by $\Delta_{\mathrm{i(k)}}$. The minimal value of $\Delta_{\mathrm{i}}$ is equal to $\Delta_{\min}$. The highest possible value of $\Delta_{\mathrm{i}}$ is represented by $\Delta_{\max}$. The distinguishing factor is $\gamma$. The consensus is 0.5.

Finding the grey relational grade (GRG) is the third step.

$$\gamma_i = \frac{1}{n}\sum_{k=1}^{n} \xi_i(k)$$

for each trial, $\gamma_i$ Represents the necessary grey relational grade, and n represents the number of response characteristics.

A representative indicator of all quality attributes, the grey relational grade shows how well the reference and comparability sequences correlate, as shown in Table 7. Combining grey relational analysis with the Taguchi technique reduces the multi-response optimization issue to a single-response optimization problem.

### 3.8 Confirmation test

A confirmation test is highly recommended to validate the experiment's results. As shown in Tables 8 and 9, the confirmation test validated the projected performance once the optimum parameters were identified. To ensure a high level of agreement between the anticipated and experimental wear loss findings, a comparison was made between the estimated

**Table 7** Grey relational analysis coefficients and grade values:

| Exp. No's: | COF | Wear-loss (g) | Grey-relation Co-efficient | | Grey relation Grades | Ranks |
|---|---|---|---|---|---|---|
| | | | **COF** | **Wear-loss (g)** | | |
| 1 | 0.1445 | 0.0085 | 0.815 | 0.608 | 0.712 | 6 |
| 2 | 0.1702 | 0.0075 | 0.532 | 0.654 | 0.593 | 10 |
| 3 | 0.1643 | 0.0098 | 0.578 | 0.558 | 0.568 | 12 |
| 4 | 0.1655 | 0.0105 | 0.568 | 0.534 | 0.551 | 15 |
| 5 | 0.1718 | 0.0105 | 0.521 | 0.534 | 0.527 | 16 |
| 6 | 0.1561 | 0.0103 | 0.657 | 0.540 | 0.599 | 9 |
| 7 | 0.1812 | 0.0096 | 0.463 | 0.565 | 0.514 | 18 |
| 8 | 0.1618 | 0.0029 | 0.600 | 1.000 | 0.800 | 3 |
| 9 | 0.1944 | 0.0119 | 0.401 | 0.492 | 0.446 | 24 |
| 10 | 0.2032 | 0.0121 | 0.368 | 0.486 | 0.427 | 25 |
| 11 | 0.1528 | 0.0203 | 0.696 | 0.333 | 0.514 | 17 |
| 12 | 0.1985 | 0.0105 | 0.385 | 0.534 | 0.459 | 21 |
| 13 | 0.2037 | 0.0087 | 0.366 | 0.600 | 0.483 | 19 |
| 14 | 0.1863 | 0.0067 | 0.437 | 0.696 | 0.566 | 13 |
| 15 | 0.1801 | 0.0145 | 0.469 | 0.429 | 0.449 | 22 |
| 16 | 0.1449 | 0.0134 | 0.809 | 0.453 | 0.631 | 8 |
| 17 | 0.1904 | 0.0162 | 0.418 | 0.395 | 0.407 | 26 |
| 18 | 0.1489 | 0.0037 | 0.747 | 0.916 | 0.831 | 1 |
| 19 | 0.1421 | 0.0112 | 0.858 | 0.512 | 0.685 | 7 |
| 20 | 0.1611 | 0.0042 | 0.606 | 0.870 | 0.738 | 4 |
| 21 | 0.1497 | 0.0042 | 0.736 | 0.870 | 0.803 | 2 |
| 22 | 0.1356 | 0.0133 | 1.000 | 0.455 | 0.728 | 5 |
| 23 | 0.1730 | 0.0081 | 0.512 | 0.626 | 0.569 | 11 |
| 24 | 0.1758 | 0.0129 | 0.494 | 0.465 | 0.480 | 20 |
| 25 | 0.1814 | 0.0073 | 0.462 | 0.664 | 0.563 | 14 |
| 26 | 0.2011 | 0.0109 | 0.375 | 0.521 | 0.448 | 23 |
| 27 | 0.2142 | 0.0161 | 0.333 | 0.397 | 0.365 | 27 |

**Table 8** S/N-ratio responses for Wear loss

| Levels | Sliding Speed (m/s) | Load (N) | Sliding Distance (m) | Reinforcement (wt. % of Gr) |
|---|---|---|---|---|
| 1 | 38.91 | 43.18 | 44.70 | 38.63 |
| 2 | 40.68 | 39.87 | 40.27 | 42.12 |
| 3 | 42.68 | 39.23 | 37.31 | 41.52 |
| Delta | 3.78 | 3.95 | 7.39 | 3.49 |
| Rank | 3 | 2 | 1 | 4 |

**Table 9** S/N-ratio responses for COF

| Levels | Sliding Speed (m/s) | Load (N) | Sliding Distance (m) | Reinforcement (wt. % of Gr) |
|---|---|---|---|---|
| 1 | 15.79 | 16.12 | 15.46 | 15.14 |
| 2 | 15.33 | 15.70 | 15.22 | 15.83 |
| 3 | 14.93 | 14.23 | 15.38 | 15.08 |
| Delta | 0.86 | 1.90 | 0.24 | 0.75 |
| Rank | 2 | 1 | 4 | 3 |

**Table 10** Confirmation test

| | Recommended optimal parameters | Initial parameters | |
|---|---|---|---|
| | Predicted or expected results | | Actual Testing results |
| | A2-B1-C2-D3 | A3-B3-C3-D3 | |
| COF | 0.15153 | 0.218 | 0.1489 |
| S/N-ratio (Db) | 16.83428 | 13.2309 | 16.5421 |
| % of change in S/N-Ratio | Recommended optimal parameters | 3.31 | |
| | A2-B1-C2-D3 | A3-B3-C3-D3 | |
| Wear-loss(g) | 0.003841 | 0.0137 | 0.0037 |
| S/N-ratio (dB) | 50.48942 | 37.2656 | 48.636 |
| % of change in S/N-Ratio | | 11.37 | |

wear loss and the experimentally obtained wear loss using the ideal parameters, as shown in Table 10. Wear loss is reduced by about 25.08% and the coefficient of friction by 54.37% as a result of an 11.37 dB and 3.31 dB improvement in the signal-to-noise ratio, respectively, between the initial test condition and the ideal testing circumstances. This study's model successfully estimated the tribological characteristics according to the findings.

### 3.9 Wear mechanisms

Microscopic graphs of the damaged surfaces (Fig. 8a–d) using scanning electron microscopy. Wear behaviour of the Al7075-5wt.% SiC composite is indicated by the wear created by deeper stable strips and the fracture of its oxide coating, leading to an increase in wear loss, as seen in the standard scanning electron micrographs of sintered samples (Fig. 8b). Evidence of cracked SiC reinforcements indicates that Al7075-5wt.% SiC was plastically deformed to a substantial degree. Figures 8c, d show that these composites exhibit moderate plastic deformation at the groove borders and more excellent patterns overall. The substrate surface is made even smoother with these graphite reinforcements. Figure 8d shows the morphology of the hybrid material Al7075-5wt.% SiC-10wt.% Gr exhibits the considerable wear features associated with the material. Wear particles were smaller on average because Graphite was spread throughout the aluminium matrix. On the flip side, the hybrid composite's wear debris had fine and coarse particles arranged in irregular patterns. The longer debris strips seen in 10 wt.% graphite composites were mostly caused by breaking reinforcement particles rather than the solid lubricant effect, as shown in 5 wt.% graphite composites. Asperities etch themselves deeply onto composite counter discs, worn debris hardens, and ploughing action creates a succession of deep grooves (Mavhungu et al. 2017; Arora et al. 2016; Madhusudan et al. 2016). When testing for wear, one critical component is the temperature rise of the sliding surfaces (Ozben et al. 2008; Yanming and Zehua 2000; Singh et al. 2022).

Figure 8 demonstrates that compared to Al7075-5 wt.% SiC-5wt.% Gr composites, the temperature increases more rapidly on worn-out surfaces of Al7075-5wt.% SiC and Al7075-5wt.% SiC-10wt.% Gr composites. This is because the former two types of composites have a higher friction coefficient at their surfaces than their counterparts. Table 5 shows that compared to the Al7075-5wt.% SiC-10wt.% Gr composite, this Al7075-5wt.% SiC-5wt.% Gr composite had a lower friction coefficient. The wear process causes a temperature rise, although these properties mitigate this effect, decreasing the adhesiveness of the composite's surface (Ozben et al. 2008; Liu et al. 2021). Furthermore, improved graphite self-lubrication reduced the wear characteristics of the damaged surface.

## 4 Conclusion

A hybrid composite material composed of Al7075, SiC, and Graphite was successfully manufactured using the powder metallurgical process in this investigation. Increasing the graphite weight percentage (between 0 and 10%) gives hybrid composites a lower hardness and density. The hybrid composites with 5% graphite by weight had the best tribological and wear behaviours. Adding graphite particles as secondary reinforcements to an aluminium 7075 matrix may improve its wear properties.

- Al7075 composites became harder as SiC wt.% grew from 0 to 5. The Al7075/5% SiC composite has higher hardness than 0% SiC composites because to its high SiC content and uniform dispersion. SiC wt.% increases hardness by 5% from 0 to 5.
- Al7075/5%SiC/Gr hybrid composites had higher hardness from 0 to 5 and lower hardness from 5 to 10. The hardness of Al7075/5% SiC/5% Gr hybrid composite increases 2.7% when graphite wt.% is increased from 0 to 5.
- In the given studies, the analysis of variance (ANOVA) showed that variables like the proportion of Graphite in the composite weight (13.31%), sliding speed (11.96%), sliding distance (55.98%), and applied force (13.31%) all affected wear loss. The composites' coefficient of friction was most affected by sliding speed (10.35%), sliding Distance (0.87%), and the applied load (61.25%), graphite reinforcement (8.7%).

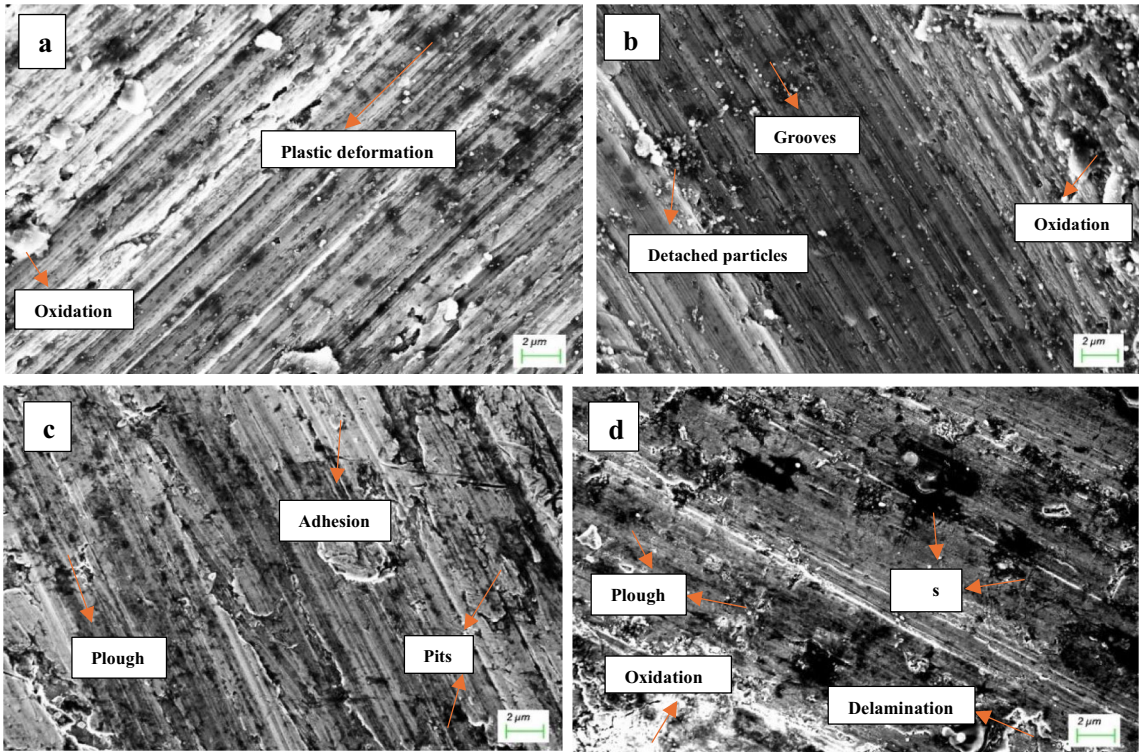


**Fig. 8** Wear morphologies: **a** Al 7075, **b** Al 7075–5 wt.% SiC-0 wt.% Gr, **c** Al 7075–5 wt.% SiC-5 wt.% Gr, **d** Al 7075–5 wt.% SiC-10 wt.% Gr

- The ideal process parameters for wear loss (A2-B1-C1-D3) and coefficient of friction (A2-B1-C1-D1) were found in a Taguchi observational study of, respectively. Consequently, there has been a 20.45 dB and 4.17 dB rise in the S/N ratio from the initial test settings to the ideal testing circumstances, with a corresponding decrease of about 45.11% in wear loss and 68.50% in friction coefficient.
- Taguchi Grey relationship analysis revealed that the confirmation test (A2-B1-C2-D3) for wear loss and COF had simultaneous optimal testing conditions that reduced wear loss by 25.08% and the friction coefficient by 54.37% compared to the initial standard results.
- The solid lubricant graphite could be included because of the protective surface coating that formed between the counter surface and the pin. Reducing the friction coefficient and enhancing wear resistance are two benefits of it.

**Author contributions** All the authors Atla Sridhar, Nagavelly Shiva Kumar, K. Prasanna Lakshmi, and CH.V. Satyanarayana Raju, planned the experiments. Corresponding authors Atla Sridhar, K. Prasanna Lakshmi, and CH.V. Raju carried out the experiments by preparing samples, conducting the experiments, interpreting the results. Atla Sridhar supervised all stages of the work and took the lead in writing and verifying the manuscript. The author's Atla Sridhar and Nagavelly Shiva Kumar discussed and contributed to the final version of the manuscript.

**Funding** This research received no specific grant from any funding agency.

**Data availability** This manuscript has no associated data.

## Declarations

**Conflict of interest** The authors declare that they have no know competing financial interests or personal relationships that could have appeared to influence the work reported in this article. The authors reported no potential conflict of interest.

## References:

Akhtar SS (2021) A critical review on self-lubricating ceramic-composite cutting tools. Ceram Int 47(15):20745–20767

Ande R, Gulati P, Shukla DK, Dhingra H (2019) Microstructural and wear characteristics of friction stir processed Al-7075/SiC reinforced aluminium composite. Mater Today Proc 18:4092–4101

Arora A, Astarita A, Boccarusso L, Mahesh VP (2016) Experimental characterization of metal matrix composite with aluminium matrix and Molybdenum powders as reinforcement. Proc Eng 167:245–251

Arunkumar S, Ashokkumar R, Sundaram MS, SukethKanna KM, Vigneshwara S (2020) Optimization of wear behaviour of Al7075 hybrid metal matrix composites using Taguchi approach. Mater Today Proc 33:570–577

Arya RK, Kumar R, Telang A (2023) Influence of microstructure on tribological behaviors of Al6061 metal matrix composite reinforced with silicon nitride (Si3N4) and silicon carbide (SiC) micro particles. SILICON 15(9):3987–4001

Basavarajappa S, Kumar NS, Shankar GS, Suresh R (2017) Some studies on mechanical and machining characteristics of Al2219/n-B4C/MoS2 nano-hybrid metal matrix composites. Measurement 107:1–11

Berman D, Erdemir A, Sumant AV (2014) Graphene: a new emerging lubricant. Mater Today 17(1):31–42

Bharathi P, Kumar TS (2023) Mechanical characteristics and wear behaviour of Al/SiC and Al/SiC/B4C hybrid metal matrix composites fabricated through powder metallurgy route. SILICON 15(10):4259–4275

Bhoi NK, Singh H, Pratap S (2020) Developments in the aluminum metal matrix composites reinforced by micro/nano particles–a review. J Compos Mater 54(6):813–833

Daver EM, Ullrich WJ, Balubhai Patel K (1988) Aluminium P/M parts-materials, production and properties. Key Eng Mater 29:401–428

Devaganesh S, Kumar PD, Venkatesh N, Balaji R (2020) Study on the mechanical and tribological performances of hybrid SiC-Al7075 metal matrix composites. J Market Res 9(3):3759–3766

Doddamani S, Kaleemulla M, Begum Y, Anand KJ (2017) An investigation on wear behavior of graphite reinforced aluminum metal matrix composites. Special Issue: J Res Sci Technol Eng Manag, NCETERM-2017, pp 1–6

Gajalakshmi K, Senthilkumar N, Prabu B (2019) Multi-response optimization of dry sliding wear parameters of AA6026 using hybrid gray relational analysis coupled with response surface method. Meas Control 52(5–6):540–553

Girish BM, Satish BM, Sarapure S, Basawaraj. (2016) Optimization of wear behavior of magnesium alloy AZ91 hybrid composites using taguchi experimental design. Metall and Mater Trans A 47:3193–3200

Gugulothu B, Selvaraj S, Varatharajulu M (2023) A retrospective investigation on hybrid metal matrix composites: materials, processing methods, and properties of composites. Iran J Chem Chem Eng 42(6):1842–1870

Gupta RK, Murty BS, Birbilis N, Gupta RK, Murty BS, Birbilis N (2017) High-energy ball milling parameters in production of nanocrystalline Al alloys. In: Gupta RK, Murty BS, Birbilis N (eds) An overview of high-energy Ball Milled nanocrystalline aluminum alloys. Springer, pp 7–28

Heard R (2021) Novel scanning electron microscope (SEM) imaging approaches to study microstructural evolution of alloys at elevated temperatures (Doctoral dissertation, University of Oxford).

Holmberg K, Matthews A (2009) Coatings tribology: properties, mechanisms, techniques and applications in surface engineering. Elsevier

Hong S, Wu Y, Wang B, Zhang J, Zheng Y, Qiao L (2017) The effect of temperature on the dry sliding wear behavior of HVOF sprayed nanostructured WC-CoCr coatings. Ceram Int 43(1):458–462

Ibrahim MF, Garza-Elizondo GH, Samuel AM, Samuel FH (2016) Optimizing the heat treatment of high-strength 7075-type wrought alloys: A metallographic study. Int J Metalcast 10:264–275

Ikubanni PP, Oki M, Adeleke AA, Agboola OO (2021) Optimization of the tribological properties of hybrid reinforced aluminium matrix composites using Taguchi and Grey's relational analysis. Sci Afr 12:e00839

Jamwal A, Seth PP, Kumar D, Agrawal R, Sadasivuni KK, Gupta P (2020) Microstructural, tribological and compression behaviour of Copper matrix reinforced with Graphite-SiC hybrid composites. Mater Chem Phys 251:123090

Kalsi NS, Singh D, Kumar J (2019) Tribological, physical and microstructural characterization of silicon carbide reinforced aluminium matrix composites: a review. Mater Today Proc 18:3218–3232

Koli DK, Agnihotri G, Purohit R (2014) A review on properties, behaviour and processing methods for Al-nano Al2O3 composites. Proc Mater Sci 6:567–589

Krishna Prasad S, Dayanand S, Rajesh M, Nagaral M, Auradi V, Selvaraj R (2022) Preparation and mechanical characterization of TiC particles reinforced Al7075 alloy composites. Adv Mater Sci Eng 2022(1):7105189

Kumar NS (2018) Mechanical and wear behavior of ZA-27/Sic/Gr hybrid metal matrix composites. Materials Today: Proceedings 5(9):19969–19975

Kumar KR, Pridhar T, Balaji VS (2018) Mechanical properties and characterization of zirconium oxide (ZrO2) and coconut shell ash (CSA) reinforced aluminium (Al 6082) matrix hybrid composite. J Alloy Compd 765:171–179

Liu Q, Wang Y, Bai Y, Li ZD, Bao MY, Zhan H, Ma YS (2021) Microstructural optimization and anti-wear performance of supersonic atmospheric plasma sprayed nickel based self-lubricating coatings under heavy load. Surf Coat Technol 421:127383

Madhusudan S, Sarcar MMM, Rao NBRM (2016) Mechanical properties of Aluminum-Copper (p) composite metallic materials. J Appl Res Technol 14(5):293–299

Manoj M, Jinu GR, Kumar JS, Mugendiran V (2022) Effect of TiB2 particles on the morphological, mechanical and corrosion behaviour of Al7075 metal matrix composite produced using stir casting process. Int J Metalcast 16:1517–1532

Mavhungu ST, Akinlabi ET, Onitiri MA, Varachia FM (2017) Aluminum matrix composites for industrial use: advances and trends. Proc Manuf 7:178–182

Mohan R, Ramesh Babu N (2011) Design, development and characterization of ice bonded abrasive polishing process. Int J Abras Technol 4(1):57–76

Ozben T, Kilickap E, Cakır O (2008) Investigation of mechanical and machinability properties of SiC particle reinforced Al-MMC. J Mater Process Technol 198(1–3):220–225

Paulraj D, Jeyakumar PD, Rajamurugan G, Krishnasamy P (2021) Influence of nano TiO2/micro (SiC/B4C) reinforcement on the mechanical, wear and corrosion behaviour of A356 metal matrix composite. Arch Metall Mater 66(3):871–880

Prasad DS, Shoba C (2014) Hybrid composites–a better choice for high wear resistant materials. J Mark Res 3(2):172–178

Rao DR, Srinivas C (2023) Influence of process parameters on microstructure and mechanical properties ofAS21-SiC composites through two-step stir-casting. SILICON 15(2):813–827

Rao VR, Ramanaiah N, Sarcar MMM (2016) Tribological properties of aluminium metal matrix composites (AA7075 reinforced with titanium carbide (TiC) particles). Int J Adv Sci Technol 88:13–26

Ravi B, Kumar AP, Naik BB, Kumar SA (2018) Production and investigation on mechanical properties of TiC reinforced Al7075 MMC. Mater Today Proc 5(9):17924–17929

Rebba B, Ramanaiah N (2014) Evaluation of mechanical properties of aluminium alloy (Al-2024) reinforced with molybdenum disulphide (MOS2) metal matrix composites. Proc Mater Sci 6:1161–1169

Rohatgi PK, Ajay Kumar P, Chelliah NM, Rajan TPD (2020) Solidification processing of cast metal matrix composites over the last 50 years and opportunities for the future. JOM 72:2912–2926

Saurabh A, Joshi K, Manoj A, Verma PC (2022) Process optimization of automotive brake material in dry sliding using taguchi and ANOVA techniques for wear control. Lubricants 10(7):161

Sawyer WG, Argibay N, Burris DL, Krick BA (2014) Mechanistic studies in friction and wear of bulk materials. Annu Rev Mater Res 44:395–427

Schneider LC (2003) Compaction and yield behaviour of particulate materials. University of Leicester (United Kingdom)

Sharma A, Tripathi A, Narsimhachary D, Mahto RP, Paul J (2019) Surface alteration of aluminium alloy by an exfoliated graphitic tribolayer during friction surfacing using a consumable graphite rich tool. Surf Topogr Metrol Prop 7(4):045015

Sijo MT, Jayadevan KR (2016) Analysis of stir cast aluminium silicon carbide metal matrix composite: a comprehensive review. Proc Technol 24:379–385

Singh S, Kumar S (2022) Corrosion behaviour of metal, alloy, and composite: an overview. Metal Matrix Compos, edn 1, pp 57–82

Singh H, Singh K, Vardhan S, Mohan S (2022) A comprehensive review on the new developments consideration in a stir casting processing of aluminum matrix composites. Mater Today Proc

Singh MK, Gautam RK (2019) Structural, mechanical, and electrical behavior of ceramic-reinforced copper metal matrix hybrid composites. J Mater Eng Perform 28:886–899

Stachowiak GB, Stachowiak GW (2001) The effects of particle characteristics on three-body abrasive wear. Wear 249(3–4):201–207

Topcu I, Gulsoy HO, Kadioglu N, Gulluoglu AN (2009) Processing and mechanical properties of B4C reinforced Al matrix composites. J Alloy Compd 482(1–2):516–521

Upadhyaya GS (1997) Powder metallurgy technology. Cambridge Int Science Publishing

Venkatesh VSS, Deoghare AB (2022) Microstructural characterization and mechanical behaviour of SiC and kaoline reinforced aluminium metal matrix composites fabricated through powder metallurgy technique. SILICON 14(7):3723–3737

Yanming Q, Zehua Z (2000) Tool wear and its mechanism for cutting SiC particle-reinforced aluminium matrix composites. J Mater Process Technol 100(1–3):194–199

Zhai W, Bai L, Zhou R, Fan X, Kang G, Liu Y, Zhou K (2021) Recent progress on wear-resistant materials: designs, properties, and applications. Adv Sci 8(11):2003739